Risk-driven responses to COVID-19 eliminate the tradeoff between lives and livelihoods

Authors:

Hazhir Rahmandad[1*], Ph.D.

MIT, Room E62-442, 100 Main St., Cambridge, MA 02142

Tse Yang Lim[1], M.S.

MIT, Room E62-441, 100 Main St., Cambridge, MA 02142

Affiliations:

[1]Massachusetts Institute of Technology, Cambridge, MA

*Corresponding Author

Hazhir Rahmandad

hazhir@mit.edu

+1-617-253-8912

Risk-driven responses to COVID-19 eliminate the tradeoff between lives and livelihoods

Abstract

Responses to the COVID-19 pandemic have been conditioned by a perceived tradeoff between saving lives and the economic costs of contact-reduction measures. We develop a model of SARS-CoV-2 transmission where populations endogenously reduce contacts in response to the risk of death. We estimate the model for 118 countries and assess the existence of a tradeoff between death rates and changes in contacts. In this model communities go through three phases – rapid early outbreaks, control through initial response, and a longer period of quasi-equilibrium endemic infection with effective reproduction number (R_e) fluctuating around one. Analytical characterization of this phase shows little tradeoff between contact reduction levels (underpinning economic costs) and death rates. Empirically estimating the model, we find no positive correlation between (log) death rates and (normalized) contact levels across nations, whether contacts are estimated based on epidemic curves or mobility data. While contact reduction levels are broadly similar across countries, expected death rates vary greatly, by two orders of magnitude (5-95 percentile: 0.03-17 deaths per million per day). Results suggest nations could significantly reduce the human toll of the pandemic without more disruption to normal social and economic activity than they have already faced.

Executive Summary

• **Problem specification**: The response to COVID-19 pandemic is dominated by a perceived tradeoff between saving lives through cutting social interactions vs. allowing those interactions to maintain economic livelihood of communities. It is, however, unclear if this tradeoff really exists.

• **Practitioner audience**: Local, regional, and national policy makers who control communities' responses to observed levels of COVID-19 transmission risk are grappling with this perceived tradeoff on a daily basis.

• **Core insight**: The perceived tradeoff is illusory. Every community will pay a similar price in contact reduction. What communities do control is the level of infection and deaths at which they are willing to bring down contacts enough to keep the epidemic from growing further.

• **Practical implications**: By becoming more responsive, effective leaders quickly bring down community's interactions in response to small numbers of cases and deaths. They can then maintain these small case counts at social interaction levels similar to other communities that experience much larger ongoing cases. Thus, there is a path to saving lives at limited excess costs.

Introduction

Is there a tradeoff between protecting lives and protecting livelihoods under the threat of a pandemic? The existence of this tradeoff seems intuitive. For example, the social distancing and lockdown measures needed to control the spread of COVID-19 have caused tremendous economic disruption (Brodeur et al. 2020, Coibion et al. 2020, McKee and Stuckler 2020). SARS-CoV-2 spreads through human interactions, so slowing down its spread should inevitably hurt economic activities that depend on those interactions.

The policy discourse around pandemic response draws on this intuition that communities have to make a tough choice: they either bring down their contacts, disrupting their economies but saving lives, or allow more normal interactions but incur more deaths. Assuming a positive correlation between deaths and economic activity, various nations and communities have adopted a range of approaches from stringent lockdowns to hands-off non-responses (Loayza 2020). The tradeoff framing also forces societies to pick winners and losers among their citizens: given the uneven distributions of both health risks (Hooper et al. 2020) and economic impacts (Loayza 2020), any course of action will leave many stakeholders unsatisfied.

In response, some have sought to better align the two goals by incorporating the economic costs of an uncontrolled outbreak, e.g. from morbidity and mortality (Cutler and Summers 2020), or the public health impacts of economic recessions (Bhuiyan et al. 2020, Douglas et al. 2020, Webb 2020). These arguments may mitigate longer-term tradeoffs but do not challenge the basic tension between near-term health and economic outcomes.

In this paper, we go a step further and propose that fundamentally, little tradeoff exists between health and economic outcomes even during the course of the epidemic. Specifically, we argue theoretically that the degree of contact reduction and by extension, disruption to economic activity that the pandemic necessitates is largely independent of the resultant levels of morbidity and mortality. Therefore, while there are significant economic costs associated with responding to a pandemic, every community has to pay those costs and they are not related to mortality outcomes. We find empirical support for this hypothesis using two data sources: 1) estimating a model of endogenous contact reduction in response to COVID-19 pandemic across 118 countries constituting 7.05 billion people. 2) Correlating mobility data against COVID-19 death rates across nations.

Risk-driven responses in models of epidemics

Understanding this potential tradeoff requires modeling how a community responds to the evolving risks of a pandemic. Classical models of epidemics, such as the Susceptible-Infectious-Recovered (SIR) model, predict that an outbreak grows exponentially, slowing down only when the susceptible population is depleted. Two stylized observations require adjustments to the basic SIR model. First, in most communities the initial wave of COVID-19 was brought under control while the vast majority of the population was still susceptible.

Second, the initial control has been followed by a long phase of steady, sometimes oscillatory, infections and deaths responsible for much of the public health and economic burden of the epidemic. These observations are best explained by accounting for individuals' and governments' responses to an ongoing pandemic. Models in public health and epidemiology often characterize those responses as a function of time (e.g. a time-based change in contact-rates); using historical data on policies adopted by governments; or as policy switches that are activated in response to risks (Flaxman et al. 2020, Kissler et al. 2020, R. Li et al. 2020b, Walker et al. 2020). These characterizations, while effective for fitting historical trajectories, do not allow for exploration of counter-factual scenarios where alternative evolutions of risks and responses do not follow historical data.

To understand the tradeoffs between social interactions and disease burden, one needs to endogenize how contact rates respond to perceived risks in a community. A few modeling studies in management and economics have taken this endogenous view using behavioral (Ghaffarzadegan and Rahmandad 2020, Struben 2020) or rational (Acemoglu et al. 2020, Farboodi et al. 2020) formalizations. These studies, however, have not addressed the tradeoff between contact rates and saving lives, which requires an empirical examination of the relationship across different communities.

Methods

Model and Predictions

We start with the classic SIR model (Murray 2002), and incorporate behavioral responses that endogenously change infectious contacts as a continuous function of perceived risk. Populations are divided into three groups: susceptible to the disease (S), infected (I), and removed from circulation due to recovery or death (R). We build our argument starting with the simplest incarnation of the model:

$$\frac{dS}{dt} = -r_I;\ \frac{dI}{dt} = r_I - r_R;\ \frac{dR}{dt} = r_R \quad (1)$$

$$r_I = \frac{\beta IS}{N} \quad (2)$$

$$r_R = \frac{I}{\tau} \quad (3)$$

The two main parameters are the infectious contacts per day per index case (β), and the average disease duration (τ). We use $S_f = \frac{S}{N}$ (with $N = S + I + R$) to denote the susceptible fraction of the population.

The expected secondary cases from an index case in a fully susceptible population is the basic reproduction number (R_0):

$$R_0 = \beta\tau \quad (4)$$

Because outbreaks in first-affected communities change behaviors in other nations, we call the empirically estimated values for R_0 *initial reproduction numbers*. Effective reproduction number (R_e) then accounts for reductions in secondary cases due to reduced susceptible fraction as the epidemic progresses:

$$R_e = \beta\tau S_f \quad (5)$$

With a constant β and an R_0 notably above one (Q. Li et al. 2020a) the basic SIR model predicts a rapid COVID-19 outbreak that infects most of a population in a few months, reaching herd immunity when a large fraction of the population has been infected with huge resultant loss of life. In practice, however, few communities have followed this uncontrolled trajectory. Instead, the initial exponential growth phase has been curtailed well before herd immunity, as behavioral and policy responses to perceived risk of death bring down daily infectious contacts per index case (β) enough to control the epidemic. As a result, few communities have depleted their susceptible populations (Rahmandad et al. 2020). Instead, in most countries, the initial outbreak and control phases have been followed by a third phase in which a large fraction of the population remains susceptible and experiences a stream of new cases and deaths, including occasional subsequent waves.

We capture this endogenous change in behaviors and policies by allowing β to go below its initial value (β_0) in response to perceived risk of death (D):

$$\beta = \beta_0 g(D) \quad (6)$$

Function *g* reflects contact rates relative to initial levels and offers a proxy for disruption to normal activities, the primary driver of the economic costs of an outbreak. *g(D)*=1 indicates no change in behaviors compared to pre-pandemic, whereas a society in full lockdown may push *g(D)* down to near zero.

Based on an empirical exploration of the delays in risk perception and response, we model perceived risk as a 2nd order Erlang distributed delay of per capita daily death rate (d_N; Equation 8) resulting from an infection fatality rate of *f*. An exponential function is used to formulate *g*:

$$d_N = \frac{f r_R}{N} \quad (7)$$

$$D(t) = \int_{k\geq 0} d_N(t-k)\frac{2}{\lambda}k^2 e^{\frac{2k}{\lambda}} dk \quad (8)$$

$$g(D) = e^{-\alpha D} \quad (9)$$

α represents the responsiveness of a community to perceived risk and λ represents the time it takes to perceive and respond to risks. α=0 recovers the basic SIR model. Higher α values indicate a community more responsive to the perceived risk of death from the disease.

In estimating the model we note that the time constant for upward vs. downward adjustment (when $D(t)<d_N(t)$ vs. $D(t)>d_N(t)$) of perceived risk and response may differ, e.g. raising alarms may happen faster than forgetting about the risks of a pandemic:

$$\lambda = \begin{matrix} \lambda_u \; if \; \mathrm{D(t)} < \mathrm{d_N(t)} \\ \lambda_d \; if \; \mathrm{D(t)} \geq \mathrm{d_N(t)} \end{matrix} \tag{10}$$

To capture changes in risk-response relationship over time (e.g. due to adherence fatigue), we also allow communities' responsiveness to perceived risk (α) to vary, starting from some initial responsiveness (α_0) and moving toward some final value (α_f), with parameters t_0 and θ affecting the timing and rapidity of the adjustment:

$$\alpha = \alpha_0 + (\alpha_f - \alpha_0)\frac{1}{1+e^{\frac{-(t-t_0)}{\theta}}} \tag{11}$$

For estimation, we predict observed infection rate as a function of observed death rates. Assuming an under-count ratio of γ_I for official to true cases and using the subscript "M" for official measures (vs. true values), we can write:

$$r_I = \frac{\beta_0 g(d_N) IS}{N} \Rightarrow \frac{r_{IM}}{\gamma_I} = \frac{\frac{\beta_0 g(d_{NM}) I_M S}{\gamma_I}}{N} \Rightarrow r_{IM} = \frac{\beta_0 g(d_{NM}) I_M S}{N} \xRightarrow{I_M(t)=\sum_{k=1}^{k=\tau} r_{IM}(t-k)}$$

$$r_{IM} = \beta_0 S_f g(d_{NM}) \sum_{k=1}^{k=\tau} r_{IM}(t-k) \tag{12}$$

Note that in this derivation we assume γ_I is not changing quickly on the timescale of disease duration τ, but could change over longer horizons. Susceptible fraction (S_f) is not directly observable because cumulative case counts are significantly under-estimating the true magnitude of the epidemic. Official death data (d_{NM}) are more reliable. We therefore estimate total cases by dividing cumulative deaths to-date by country-specific infectious fatality rates (f) calculated based on age-specific fatalities (Verity et al. 2020) and correcting with γ_D for country-specific under-reporting and over-estimation of f (details in S2):

$$S_f(t) = 1 - \frac{\gamma_D}{f} \sum_{s=0}^{s=t} d_{NM}(s) \tag{13}$$

Combining equations 8-13 leads to our primary estimation equation:

$$E(r_{IM}(t)) = \beta_0(1 - \frac{\gamma_D}{f}\sum_{s=0}^{s=t} d_{NM}(s))e^{-\left(\alpha_0+(\alpha_f-\alpha_0)\frac{1}{1+e^{\frac{-(t-t_0)}{\theta}}}\right)\left(\int_{s\geq 0} d_{NM}(t-s)\frac{2}{\lambda}s^2 e^{\frac{2s}{\lambda}}ds\right)}\sum_{k=1}^{k=\tau} r_{IM}(t-k) \quad (14)$$

Full model documentation is available in online appendix S5.

Quasi-equilibrium phase and its features

Risk-driven responses create a balancing feedback loop that can control the epidemic before herd immunity is reached: deaths increase while R_e>1, raising alarms and bringing down infectious contacts. R_e<1 reduces deaths until the diminishing perceived risk leads to relaxation of responses, pushing R_e up. Behavioral risk response thus creates a self-correcting process through which R_e converges to approximately one, resulting in a quasi-equilibrium phase where cases and infections are close to stable (Figure 1). The $R_{e\sim}$= ~1 condition governs changes in contacts during quasi-equilibrium phase (g_{eq})

$$R_e = 1 \Rightarrow g_{eq}(D) = \frac{1}{\beta_0 \tau S_f} = \frac{1}{R_0 S_f} \quad (15)$$

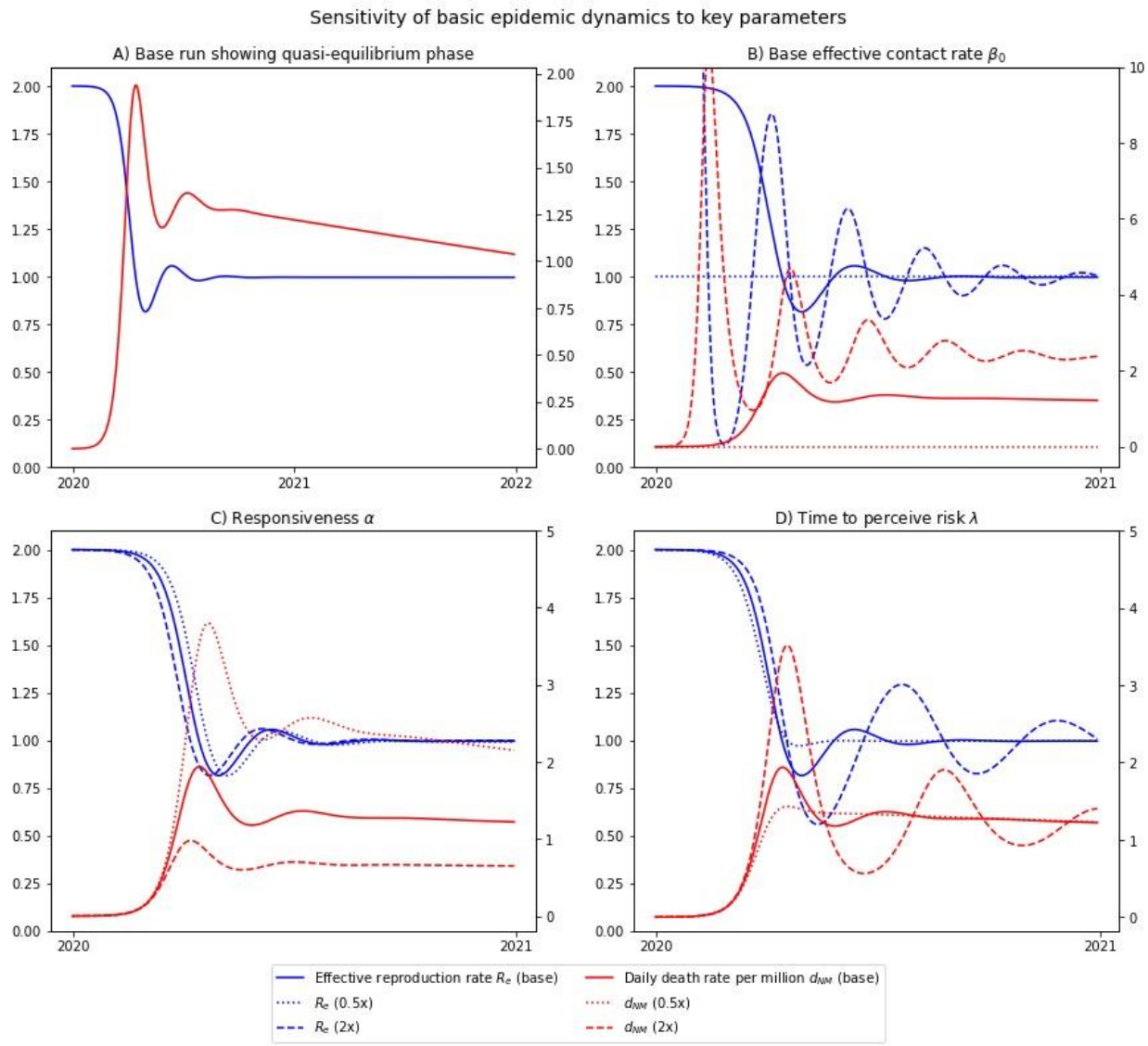

Figure 1 - R_e (left axes, blue) and daily deaths per million (right, red) in epidemics with endogenous response to risk. A) Illustrative case with β_0=2, α=0.5, and λ=15 days, f=0.5% absent vaccine quasi-equilibrium extends from mid-2020 to beyond 2022. B-D) sensitivity to variations in parameter values (0.5x and 2x base values).

This phase is a 'quasi-'equilibrium as an ongoing stream of new cases continues to reduce the susceptible fraction. Moreover, the delays between infection, death, and response may allow transmission and deaths to go higher/lower than equilibrium when rising/falling. Thus, depending on the risk-response delays (λ), communities converge to quasi-equilibrium expected death rates, d_{NM}^{eq}, or oscillate around this value (Figure 1). In that neighborhood, D(t) will on average be close to d_{NM} (equation 8), allowing us to calculate the quasi-equilibrium death rates:

$$d_{NM}^{eq} = \frac{\ln(R_0 S_f)}{\alpha} \tag{16}$$

This phase ends when S_f falls below $1/R_0$. As long as communities are responsive enough to risk to bring the initial outbreak under control, the d_{NM} values remain close to d_{NM}^{eq} and g close to g^{eq} for an extended period, making the quasi-equilibrium phase critical in the overall impact of the pandemic.

We focus on two features of the quasi-equilibrium phase. First, the normalized contact level in this phase, $g^{eq}(D)$ does not depend on the functional form or parameters of risk perception and response, nor on the number of infectious individuals (I) (See equation 15). It is simply a function of the initial reproduction number (R_0) and the susceptible fraction (S_f), which determine the contact reduction needed for $R_e \approx 1$. Second, the death rate in the quasi-equilibrium phase will depend primarily on α (along with differences in R_0 across communities). Our model predicts limited variation in normalized contacts across communities because variations in both R_0 and S_f are limited. On the other hand, differences in equilibrium death rates may be much larger, depending on empirically observed variations in responsiveness α. Finally, the correlation between d_{NM}^{eq} and g_{eq} is predicted to be non-positive, contrary to the intuitively expected tradeoff. If anything, a negative correlation may emerge if countries vary significantly in R_0 (and S_f): those with larger R_0 will have both larger d_{NM}^{eq} and smaller g_{eq}. Next, we test these hypotheses by using COVID-19 infections and mortality data to quantify the response functions and the projected quasi-equilibrium death rates across 118 countries. To provide a separate test of our hypotheses, we also look at the correlation between mobility data and death rates.

Data and Estimation

We use equation 14 to find the posterior distribution of each country's parameters ($\beta_0, \alpha_0, \alpha_f, t_0, \theta, \lambda_u, \lambda_d, \gamma_D$), using a Markov Chain Monte-Carlo method (Vrugt et al. 2009) starting with uninformed priors (details in S1). To accommodate heteroskedasticity and fat tails, we represent observed cases (r_{TM}) using a Negative Binomial distribution, which introduces a scale parameter (ϵ). We specify the average disease duration (τ) at 10 days (He et al. 2020), constant across all countries (and find limited sensitivity in the results to plausible alternative values, see S4).

We use a panel of daily data on confirmed cases and deaths for 118 countries comprising 7.05 billion people, covering dates from 31 December 2019 to 02 December 2020. We use 7-day rolling averages on this data to smooth out weekly reporting cycles and better reflect underlying trends. For mobility we use Google's COVID-19 Community Mobility Reports, which track changes in visits to different categories of destinations compared to pre-COVID-19 travel patterns based on cellphone data. All data come from the OurWorldInData global COVID-19 database (Roser et al. 2020), which aggregates its data from various official sources as well as Google's mobility reports.

Results

This simple model replicates the diverse range of trajectories observed in the epidemic thus far (Figure 2; See S3 for full sample). Over the full sample of 118 countries, R^2 for infections against data is 0.936, while the mean absolute errors normalized by mean (MAEN) are 13.2%. For a handful of countries (Argentina, Jordan, Oman) S_f falls below $1/R_0$ in our analysis period so quasi-equilibrium no longer holds; those countries are excluded henceforth.

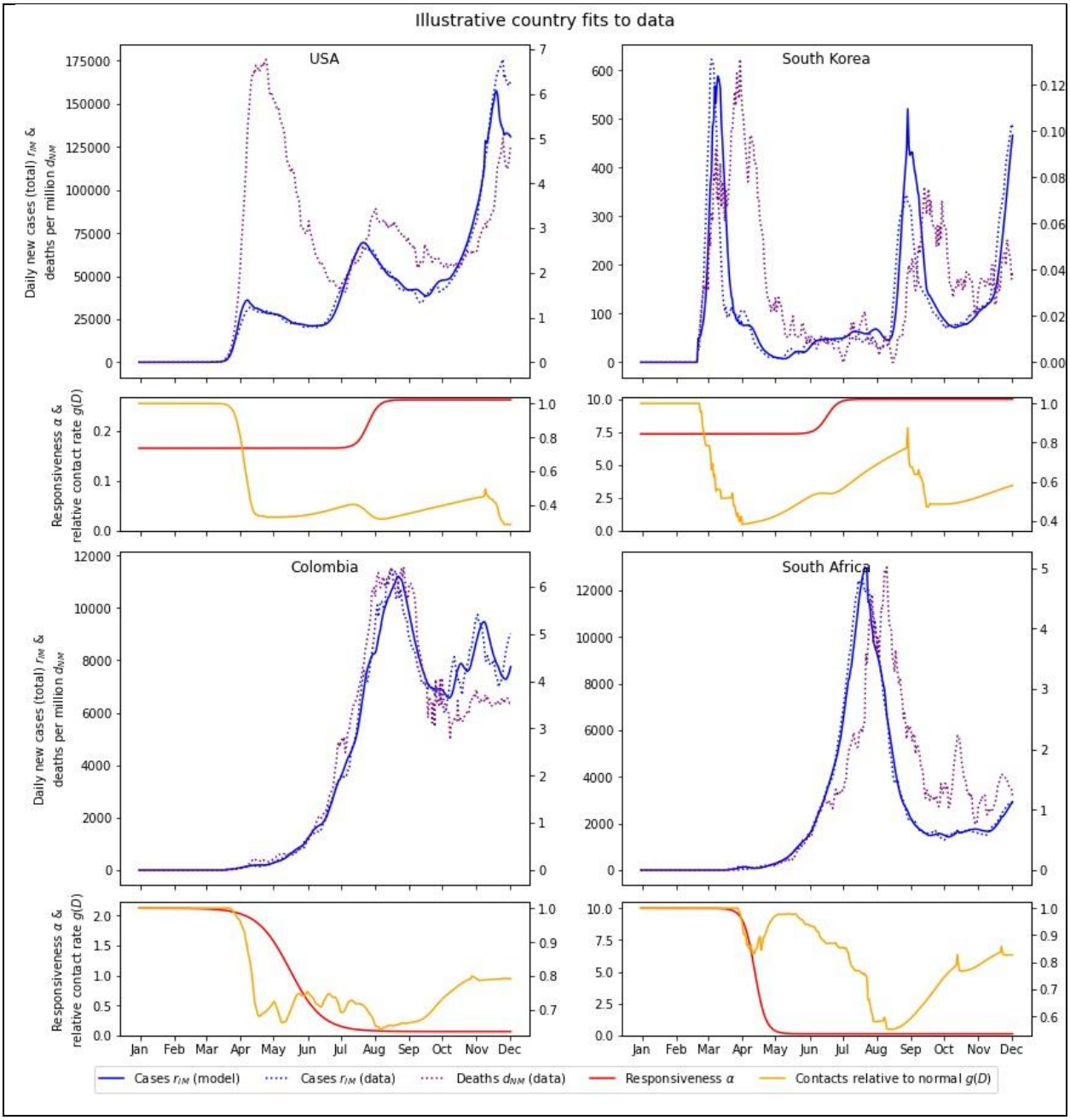

Figure 2-Sample country-specific trajectories. Daily cases (estimated and actual) are on left axis, and deaths (per million) on the right. Lower panels show α (red; left axis) and normalized contacts, g (yellow; right axis).

On average, responsiveness decreases over time: On 01 May 2020 the median effect of 1 daily death per million was to reduce contacts to 30.4% of normal, but by 02 December 2020 normalized contacts only drop to 77.7% in the same scenario. The drop in α results in increasing quasi-equilibrium death rates over time (See equation 16). There is also much variance in these response factors – in the 1 daily death per million scenario, estimated contact rates on 02 December 2020 range from 0.01%-98.3% (5th-95th percentile) of normal. As hypothesized, risk adjustment is asymmetric, with most countries increasing perceived risk much faster (median λ_u= 8.9 days) than reducing it (median λ_d= 61 days).

In most countries, quasi-equilibrium conditions hold as reproduction number remains close to one. Across these 115 countries, the R_e averaged over the last 180 days (05 June 2020-02 December 2020) has a median of 1.10 with a tight range (0.97-1.26, 5th-95th percentile) (Figure 3). In contrast, the median reported deaths (d_{NM}) averaged over the same period is 0.73 per million per day with a 5th-95th percentile range spanning 0.02-3.19. While R_e values are clustered around 1, death rates vary by over two orders of magnitude.

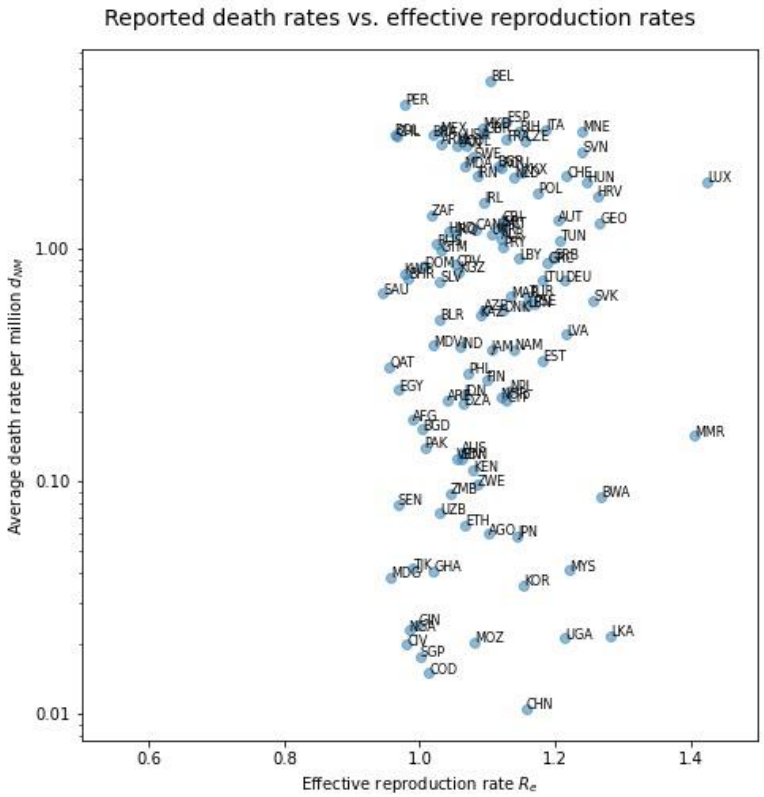

Figure 3 –Reported death rates (daily; per million) vs. estimated effective reproduction rates (R_E), both averaged over the last 180 days.

Figure 4 shows how the model's predicted quasi-equilibrium deaths compare with actual data. For each day we regress (log-transformed) observed death rates (d_{NM}) for all countries against the estimated most likely $\log(d_{NM}^{eq})$ values for that day. We then graph the estimated coefficient for these regressions over time. After a less stable early phase, the coefficient converges to the neighborhood of one and remains there, showing that d_{NM}^{eq} reliably predicts the actual reported deaths for much of the pandemic's history. This result is notable because we did not estimate death rates directly: the projected equilibrium deaths rely on the analytical derivations and the estimated behavioral parameters for risk response, and yet those analytically derived values predict reported deaths with a coefficient close to 1.

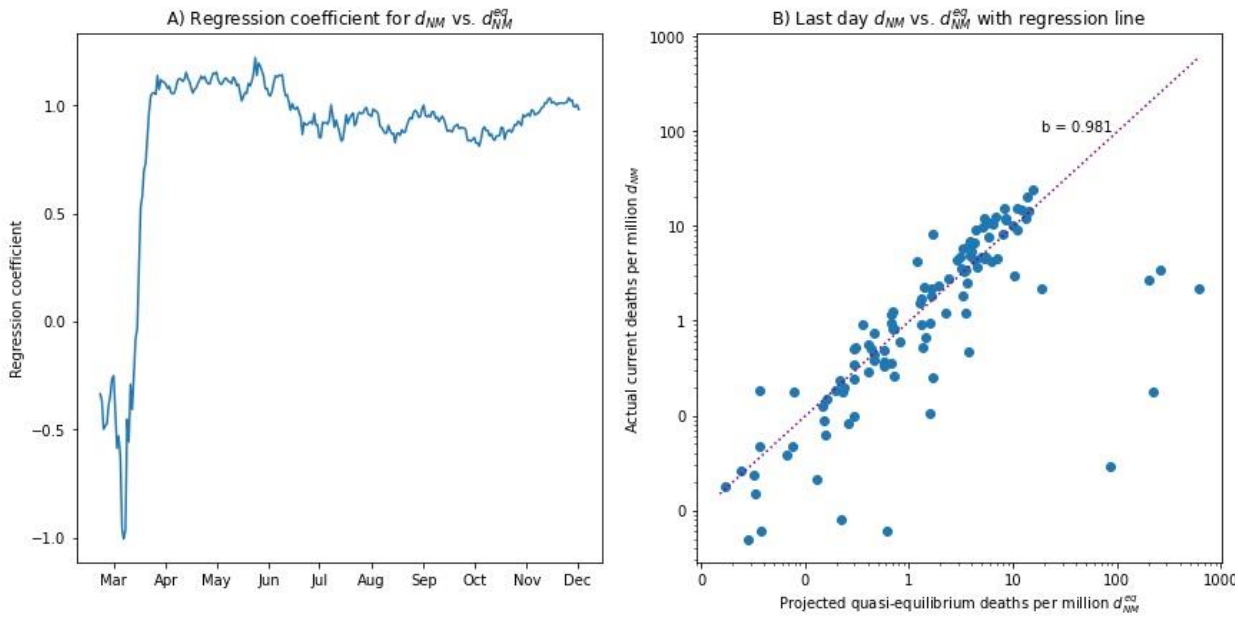

Figure 4 – Predicting reported deaths based on quasi-equilibrium calculations (using robust regression with no intercept). A) Coefficients for regressing daily death data on analytically derived quasi-equilibrium death rates. B) Scatter-plot for the two variables over the last day of data, also showing the regression line for the last coefficient in A.

Our key hypothesis informs the relationship between normalized contact levels and equilibrium death rates across nations. We assess this relationship both through our estimates and direct observations.

Figure 5A presents the scatterplot of the model estimates for the two at the end of estimation period. End-date quasi-equilibrium daily death rates (d_{NM}^{eq}) vary widely (median: 1.46; 5th-95th percentile range of 0.03 to 17; larger than past-six-month average deaths shown in Figure 3 due to declining α). In contrast, normalized contacts in this phase are much less variable with median g^{eq} of 0.690 (0.521-0.867, 5th-95th percentile). The estimates of contact rates are highly precise – the median of the interquartile ranges of each country's credible interval, normalized by its estimated value (MNIQR), is 0.057. Credible intervals on projected death rate are

wider but still fairly precise (MNIQR = 0.16). Notably, we find no positive correlation between death rate and contact rates (Pearson's r = -0.077, p = 0.411; for $\log(d_{NM}^{eq})$, r = -0.241, p = 0.009).

Figure 5B uses direct observations to inform this relationship. For deaths we use the official death tolls averaged over 180 days from 05 June 2020-02 December 2020 (as in Figure 3). To approximate contact rates relative to normal, we utilize mobility data from the Google Community Mobility database. Among others, this database uses mobile data to quantify percent changes in daily visits to *Retail and Recreation* as well as *Workplace* locations, compared to pre-pandemic rates. Using the average of these two metrics over the 180-day pre-estimation period we create a combined measure of reductions in contact which we graph against (log) deaths (See S3 for separate graphs). Again, we find a negative correlation between deaths and relative daily visits to workplaces (-0.516, p = 1.01E-07) or retail and recreation venues (-0.249, p = 0.016).

Overall, both in data (Figure 3 and Figure 5B) and in estimates (Figure 5A), we find no tradeoff between contact levels and death rates across nations; if anything, countries with lower death rates have also benefited from more limited contact reductions.

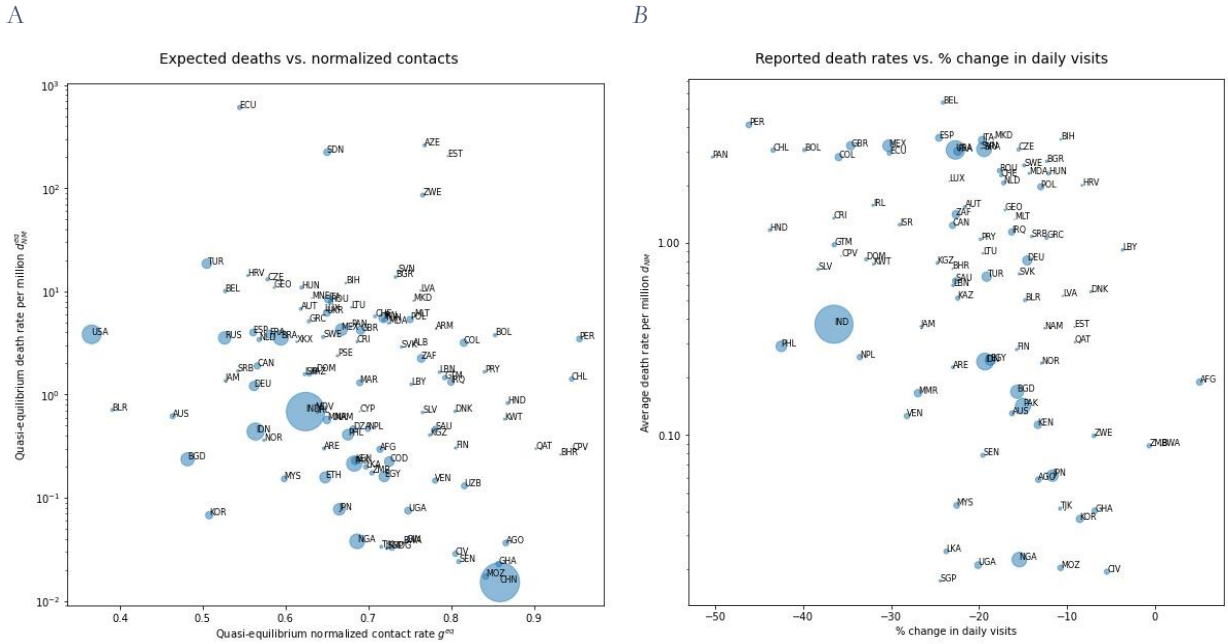

Figure 5 – Scatterplots of death rates per million (Y-axis) against contact levels normalized to pre-pandemic levels (X-axes) for model estimates and data. Size of circles scales with population. A) quasi-equilibrium daily death rates per million and normalized contact levels estimated for 02 December 2020. The few countries with very high (> 100) d_{NM}^{eq} may face large outbreaks and transition out of equilibrium

rather than actually experiencing those death rates. B) daily death rates per million against change in daily visits to workplaces and retail & recreation venues relative to pre-pandemic levels, averaged over the last 180 days.

By December 2020, α and thus the expected deaths become largely stable, but a few countries show notable changes (in both directions). Figure 6 quantifies those trends as daily fractional change in d_{NM}^{eq} at the end of the estimation period. Countries on the left of the graph are at risk of increasing equilibrium death rates in the coming weeks, a warning call to shore up responsiveness to avoid costly, and pointless, rebounds until vaccination controls the pandemic over the longer term.

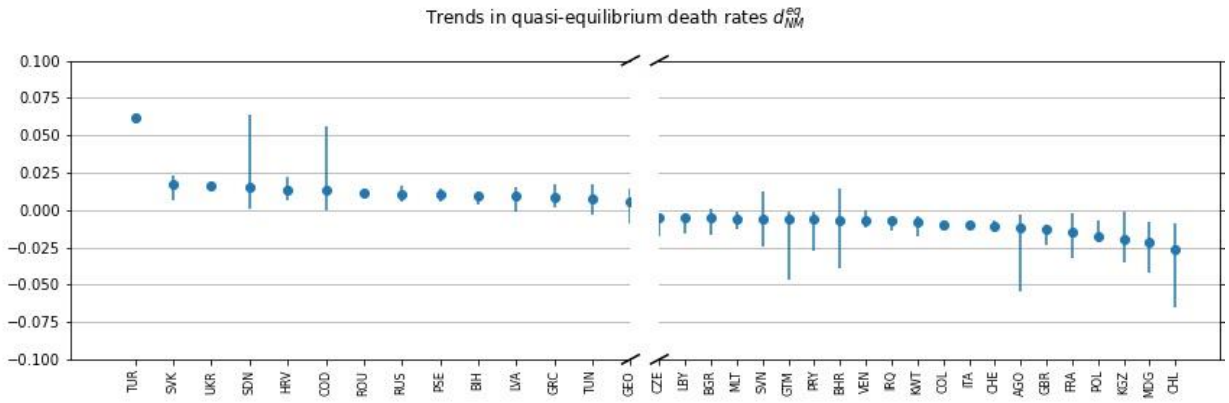

Figure 6 – Daily fractional change in d_{NM}^{eq} averaged over last 14 days (medians and 90% credible intervals). Graph limited to countries with absolute daily rates of change >0.5%. Turkey is an outlier due to a recent change in its reporting of infections.

Discussion

Our results do not directly assess the economic costs of COVID-19 pandemic, which are real and large (Baker et al. 2020, Brodeur et al. 2020, Cutler and Summers 2020). However, contrary to the tradeoff between protecting lives and minimizing disruptions that many assume, we found no positive correlation (r = -0.241, p = 0.009) between (log) death rates and (normalized) contact levels in quasi-equilibrium conditions across 115 nations. Furthermore, while contact reduction levels are broadly similar across countries (90% of countries fall between 0.521-0.867 times their initial contact rates), expected death rates vary greatly, by over two orders of magnitude (90% of countries between 0.03-17 deaths per million per day). These patterns are robust whether we estimate contact levels based on epidemic curves or use direct mobility data.

What accounts for the counterintuitive disconnect between contact reduction and death rates? Few countries tolerate exponentially growing outbreaks and deaths for long. Whether through formal policy responses or informal behavioral changes, steps will be taken to curb the epidemic, bringing down R_e to the neighborhood

of one. Across countries the contact reduction needed for reaching this reproduction number is largely similar, despite some inevitable variation as physical and cultural conditions create some differences in R_0 among countries. Communities thus suffer broadly comparable disruptions in terms of contact reduction. In contrast, the death rate a country faces in the quasi-equilibrium phase depends primarily on the country's responsiveness to risk. High responsiveness means that even slight upticks in the death rate will trigger a rapid response, bringing down R_e to 1. Low responsiveness requires higher death rates before R_e is pushed down to 1. So far countries have varied by two orders of magnitude in the death rates required to trigger this stabilizing response.

This result offers an important policy insight. Communities could experience vastly lower death rates with comparably stringent contact-reduction measures (i.e. those leading to R_e~1), if they first brought down infections to very low levels and responded quickly and vigilantly to keep R_e~1 thereafter. Other, more complex models have also noted this (lack of a) tradeoff. For example, Ferguson and colleagues (Ferguson et al. 2020) found that different trigger thresholds for re-implementing lockdowns would result in differing mortality levels but with virtually no change in the total time spent in lockdown.

Our simple model was designed primarily for investigating the tradeoffs between contact reduction and deaths and includes several limitations. One set of extensions may model the epidemic in more detail. For example, one could more explicitly model under-reporting processes, use testing data to inform the analysis, account for changing fatality rates over time, and couple model parameters across nations in a hierarchical Bayesian framework. A second set of extensions could focus on better representation of various policies and economic costs. We do not differentiate between policies used to reduce contact rates (e.g. contact tracing, isolation of vulnerable groups, school closures, masks, etc.). Some policies are more efficient in reducing contacts with less overall disruption to social life and economic activity (Benzell et al. 2020, Han et al. 2020). With effective policy sets, some nations may better maximize economic activity given the limited contact 'budget' they have based on R_e~1 condition. Another valuable extension would be to use economic output data to more directly test the predicted (lack of) tradeoff between saving lives and maintaining economic activities.

A third line of further research could explore the intriguing possibility that better economic outcomes may actually coincide with fewer deaths (Correia et al. 1918, Hasell 2020). Our analysis hints at this possibility, as we find a negative correlation between deaths and normalized contacts. Part of this negative correlation is mechanical: for a given level of responsiveness, communities with higher R_0 would have to bring down their contacts more and will have higher equilibrium death rates. However, more interesting mechanisms may be at play as well. It is possible that by keeping infections low, communities can use extensive testing, contact tracing, and isolation to control the epidemic with minimal economic disruption and also offer much better

care to those infected, options not available to those struggling with large caseloads. Limited caseloads provide policy makers with room to design better strategies and implement them with less urgency, enhancing effectiveness. Moreover, success in controlling the pandemic could also build trust between policy makers and citizens, enhancing adherence to various protocols and enabling fine-tuned individual responses which obviate the need for heavy-handed interventions such as lock-downs.

Overall, the tradeoff between lives and livelihoods has dominated policy and popular discourse around COVID-19, but focusing on this tradeoff misses a more fundamental truth. COVID-19 is a deadly disease, and whether by choice or by the force of crippling death tolls, societies will have to bring down interactions enough to contain its spread. What we control is the severity of death toll required to compel us to act. Outbreaks will grow as far as we are willing to let them, and swift reactions will save both lives and livelihoods.

Data Sharing

No data were collected specifically for this study; all data are from publicly available databases. All data-processing and analysis code, as well as the full model, its associated files, and results files, are available online at https://github.com/tseyanglim/CovidRiskResponse.

References

Acemoglu D, Chernozhukov V, Werning I, Whinston MD (2020) Optimal targeted lockdowns in a multi-group SIR model. *NBER Working Paper* 27102.

Baker SR, Bloom N, Davis SJ, Kost K, Sammon M, Viratyosin T (2020) The unprecedented stock market reaction to COVID-19. *The Review of Asset Pricing Studies* 10(4):742-758.

Benzell SG, Collis A, Nicolaides C (2020) Rationing social contact during the COVID-19 pandemic: Transmission risk and social benefits of US locations. *Proc Natl Acad Sci U S A* 117(26):14642-14644.

Bhuiyan AI, Sakib N, Pakpour AH, Griffiths MD, Mamun MA (2020) COVID-19-related suicides in Bangladesh due to lockdown and economic factors: case study evidence from media reports. *International Journal of Mental Health and Addiction*.

Brodeur A, Gray DM, Islam A, Bhuiyan S (2020) A Literature Review of the Economics of COVID-19.

Coibion O, Gorodnichenko Y, Weber M (2020) The cost of the covid-19 crisis: Lockdowns, macroeconomic expectations, and consumer spending. Report.

Correia S, Luck S, Verner E (1918) Pandemics depress the economy, public health interventions do not: Evidence from the 1918 flu. *Public Health Interventions do not: Evidence from the*.

Cutler DM, Summers LH (2020) The COVID-19 pandemic and the $16 trillion virus. *Jama* 324(15):1495-1496.

Douglas M, Katikireddi SV, Taulbut M, McKee M, McCartney G (2020) Mitigating the wider health effects of covid-19 pandemic response. *BMJ* 369:m1557.

Farboodi M, Jarosch G, Shimer R (2020) Internal and external effects of social distancing in a pandemic. Report.

Ferguson N, Laydon D, Nedjati-Gilani G, Imai N, Ainslie K, Baguelin M, Bhatia S, Boonyasiri A, Cucunubá Z, Cuomo-Dannenburg G (2020) Report 9: Impact of non-pharmaceutical interventions (NPIs) to reduce COVID19 mortality and healthcare demand. *Imperial College London* 10:77482.

Flaxman S, Mishra S, Gandy A, Unwin HJT, Mellan TA, Coupland H, Whittaker C, et al. (2020) Estimating the effects of non-pharmaceutical interventions on COVID-19 in Europe. *Nature*.

Ghaffarzadegan N, Rahmandad H (2020) Simulation-based estimation of the early spread of COVID-19 in Iran: actual versus confirmed cases. *Syst Dyn Rev* 36(1):101-129.

Han E, Tan MMJ, Turk E, Sridhar D, Leung GM, Shibuya K, Asgari N, et al. (2020) Lessons learnt from easing COVID-19 restrictions: an analysis of countries and regions in Asia Pacific and Europe. *Lancet* 396(10261):1525-1534.

Hasell J (2020) Which countries have protected both health and the economy in the pandemic. *Our World in Data* 1.

He X, Lau EHY, Wu P, Deng X, Wang J, Hao X, Lau YC, et al. (2020) Temporal dynamics in viral shedding and transmissibility of COVID-19. *Nat Med* 26(5):672-675.

Hooper MW, Nápoles AM, Pérez-Stable EJ (2020) COVID-19 and racial/ethnic disparities. *Jama*.

Kissler SM, Tedijanto C, Goldstein E, Grad YH, Lipsitch M (2020) Projecting the transmission dynamics of SARS-CoV-2 through the postpandemic period. *Science* 368(6493):860-868.

Li Q, Guan X, Wu P, Wang X, Zhou L, Tong Y, Ren R, et al. (2020a) Early Transmission Dynamics in Wuhan, China, of Novel Coronavirus-Infected Pneumonia. *N Engl J Med* 382(13):1199-1207.

Li R, Pei S, Chen B, Song Y, Zhang T, Yang W, Shaman J (2020b) Substantial undocumented infection facilitates the rapid dissemination of novel coronavirus (SARS-CoV2). *Science*.

Loayza NV (2020) Costs and Trade-Offs in the Fight Against the COVID-19 Pandemic: A Developing Country Perspective. World Bank.

McKee M, Stuckler D (2020) If the world fails to protect the economy, COVID-19 will damage health not just now but also in the future. *Nature Medicine* 26(5):640-642.

Murray JD (2002) *Mathematical biology*, 3rd ed. (Springer, New York).

Rahmandad H, Lim TY, Sterman J (2020) Estimating COVID-19 under-reporting across 86 nations: implications for projections and control. *Available at SSRN 3635047*.

Roser M, Ritchie H, Ortiz-Ospina E, Hasell J (2020) Coronavirus pandemic (COVID-19). *Our World in Data*.

Struben J (2020) The coronavirus disease (COVID-19) pandemic: simulation-based assessment of outbreak responses and postpeak strategies. *Syst Dyn Rev*.

Verity R, Okell LC, Dorigatti I, Winskill P, Whittaker C, Imai N, Cuomo-Dannenburg G, Thompson H, Walker PG, Fu H (2020) Estimates of the severity of coronavirus disease 2019: a model-based analysis. *The Lancet infectious diseases*.

Vrugt JA, Ter Braak C, Diks C, Robinson BA, Hyman JM, Higdon D (2009) Accelerating Markov chain Monte Carlo simulation by differential evolution with self-adaptive randomized subspace sampling. *International Journal of Nonlinear Sciences and Numerical Simulation* 10(3):273-290.

Walker PGT, Whittaker C, Watson OJ, Baguelin M, Winskill P, Hamlet A, Djafaara BA, et al. (2020) The impact of COVID-19 and strategies for mitigation and suppression in low- and middle-income countries. *Science*.

Webb L (2020) Covid-19 lockdown: a perfect storm for older people's mental health. *Journal of psychiatric and mental health nursing*.

Online Appendix to Accompany:

Risk-driven responses to COVID-19 eliminate the tradeoff between lives and livelihoods

Contents

S1 – Estimation method 2

S2 – Data processing 2

IFR calculation 3

S3 – Full results 4

S4 – Sensitivity results 7

Disease Duration 8

Estimation without behavioural response 11

S5 – Model equations listing 12

References 13

S1 – Estimation method

The estimation equation for our model (equation 14 in the main paper) is replicated below:

$$E\big(r_{IM}(t)\big) =$$

$$\beta_0\left(1-\frac{\gamma_D}{f}\sum_{s=0}^{s=t} d_{NM}(s)\right)e^{-\left(\alpha_0+(\alpha_f-\alpha_0)\frac{1}{1+e^{\frac{-(t-t_0)}{\theta}}}\right)\left(\int_{s\geq 0} d_{NM}(t-s)\frac{2}{\lambda}s^2 e^{\frac{2s}{\lambda}}ds\right)}\sum_{k=1}^{k=\tau} r_{IM}(t-k)$$

This equation predicts the expected number of new infections for day t as a function of past infections (to calculate stock of infectious individuals) and past death rates (to calculate the response function). We assume the observed infections follow a negative binomial distribution with the given mean from this equation and a scale parameter, ϵ, that is estimated to replicate observed error distributions. The negative binomial distribution provides the flexibility to account for heteroscedasticity, over-dispersion, and fat tails, allowing a robust estimation despite substantial randomness in the data-generating process.

The model includes the following unknown parameters: $\boldsymbol{\omega} = [\beta_0, \alpha_0, \alpha_f, t_0, \theta, \lambda_u, \lambda_d, \gamma_D, \epsilon]$ – 4 $(\alpha_0, \alpha_f, t_0, \theta)$ quantify responsiveness and how it changes over time, 2 (λ_u, λ_d) specify the risk perception delays, β_0 estimates the initial rate of infectious contacts per day per index case, and γ_D estimates the potential under-valuation of Infection Fatality Rates (*f* values) for each country . Besides the f values (see IFR calculation below for details) the model includes two other given parameters, the duration of disease (10 days) and the order of the perception delay (2).

More compactly, the model yields a (log)likelihood for observing the daily reported cases $(r_{IM}(t))$, given a vector of unknown model parameters $\boldsymbol{\omega}$ and the reported daily cases and death rate for each country prior to the current date $(d_{NM}(t-))$ and $r_{IM}(t-))$: $LL_{NegBin}(r_{IM}(t)|\boldsymbol{\omega}, r_{IM}(t-), d_{NM}(t-))$

The estimation process seeks to identify the values for $\boldsymbol{\omega}$ that maximise this likelihood or are likely to be observed given that peak.

We estimate the model separately for each country. Separating countries significantly speeds up estimation and makes it feasible to conduct the full analysis within days on a 48-core server. For each country, we estimate the parameter vector $\boldsymbol{\omega}$ using the Powell direction search method implemented in Vensim™ DSS simulation software, restarting the optimization at 20 random points in the feasible parameter space. From the resulting optimum, we use MCMC to explore the payoff landscape to identify the high-likelihood region of parameter space. The MCMC algorithm used is designed for exploring high-dimensional parameter spaces; for more details see (Vrugt et al. 2009). We draw a total of 500000 samples for each country, of which the first 300000 are discarded (the burn-in period); by the end of the burn-in, the chains are well-mixed and stable (Gelman-Rubin PSRF statistic < 1.1). We use the remaining 200000 samples to derive credible intervals for parameter and outcome estimates.

S2 – Data processing

Data on daily confirmed cases and deaths come from the OurWorldInData (OWID) global COVID-19 database (Roser et al. 2020), which draws on the Johns Hopkins University CSSE COVID

dashboard (Dong et al. 2020). The CSSE dashboard in turn aggregates its data primarily from official sources such as the US Centres for Disease Control and Prevention (CDC), the European CDC, the World Health Organization, and national health ministries, updating at least daily.

We use OWID's 7-day rolling averages for new cases ('new_cases_smoothed') and deaths per million population ('new_deaths_smoothed_per_million'). COVID-19 case and death reporting data show strong weekly cycles in many countries, as well as occasional anomalous spikes due to e.g. irregularities in test reporting or redefinitions by government statistical agencies; using the rolling average data smooths out these cycles, which we are not attempting to model here, to better reflect underlying trends.

Our analysis includes all countries in the dataset with at least 10000 cumulative cases reported, and at least 20 days of data. We exclude countries with fewer than 10000 cumulative cases to avoid skewing the results with outliers. The minimum datapoint requirement helps ensure robust estimation. In total, 118 countries meet these criteria as of 02 December 2020.

For countries included, we utilise data starting from the date when they exceed 100 cumulative cases reported. Excluding early data entails a tradeoff. Excluding it makes estimating the true basic reproduction number (R_0) more difficult – as discussed in the main text, after forceful outbreaks in the first countries, most others adopted various precautions that brought down R_0 below its pre-pandemic level. Furthermore, excluding the early data may cut out the initial dynamics of infection. As a result, our estimated values for initial reproduction number are likely underestimates of basic reproduction number, and thus the g estimates may tend to be larger than the true changes in the contact rates compared to pre-pandemic levels. On the other hand, many of the early cases reported in most countries were due to travellers, and often identified and isolated early on. The data during this earliest 'importation' stage therefore do not accurately reflect community transmission dynamics we are modelling. Rapid changes in the testing coverage also impact our ability to use assume ascertainment rates are stable in the τ time horizon as needed in our derivations (see equation 12 in the main text). We selected the 100 case cut-off to balance reasonably estimating R_0 with correctly reflecting transmission dynamics rather than travel networks, which are out of scope for this model.

For mobility data we use Google's COVID-19 Community Mobility Reports (https://www.google.com/covid19/mobility). We access this data as compiled by OWID (https://ourworldindata.org/covid-mobility-trends) which provides consistent mapping for country names to other data we use.

Data are downloaded and processed with Python 3 code, using Pandas and NumPy packages. For the full data processing code, see https://github.com/tseyanglim/CovidRiskResponse.

IFR calculation

Most countries' reported case counts substantially under-estimate the true magnitude of the epidemic (Rahmandad et al. 2020). To estimate the remaining susceptible fraction (S_j) for each country over time, we therefore rely on reported deaths, which while still variable are more reliable, multiplying cumulative reported deaths by an estimated country-specific under-reporting ratio (γ_D) and using country-specific infection fatality rates (IFR) to calculate cumulative infections.

Age strongly influences IFR, with older patients far more likely to die of COVID-19 (Verity et al. 2020). We therefore calculate country-specific IFRs based on each country's age structure.

We use data from the World Bank's World Development Indicators (World-Bank 2014) on the age distribution of each country's population in 10-year age strata to calculate an age-weighted average of the IFRs for COVID patients by 10-year age group estimated in (Verity et al. 2020). The resulting demography-adjusted country-specific IFRs range from 0.14% (Uganda) to 1.51% (Japan), with a mean of 0.54% and median of 0.44% (Lebanon). For the handful of countries for which up-to-date demographic data are unavailable, we use a baseline IFR of 0.50%.

We incorporate an estimated multiplier for actual to calculated deaths, γ_D, to account for potential undercounts of death and reductions in IFR compared to early values estimated from the methods we used. In estimation we restrict this multiplier to be between 1 and 4.

S3 – Full results

Figure S1 shows fits to data for simulated infection rates for all 118 countries. Blue lines show model-generated daily infection rates, while red lines show 7-day rolling average infection rates from OWID. The correspondence between model and data is very close for most countries, with a few outliers bringing down the quality of fit a bit; yet over the full sample of 118 countries, R^2 for infections against data is 0.936, while the mean absolute errors normalized by mean (MAEN) are 13.2%. The quality of fit should not come as a total surprise: the model uses infection rates from the past 10 days to predict current-day infections, and thus to the extent that infections are auto-correlated, the estimation process can use this anchor to offer close approximations for the number of new cases. However, the behavioural response function does add significant value in terms of quality of fit, which we demonstrate in the sensitivity analysis section by comparing results against estimates that do not account for behaviour responses.

Table S1 summarises estimated parameter values across the 115 countries which met the quasi-equilibrium condition ($S_f > 1/R_0$). 3 of the 118 total countries estimated (ARG: Argentina, JOR: Jordan, OMN: Oman) no longer meet this condition as of 02 December 2020, and were excluded from further analyses. For the full table of country-by-country parameter estimates, see https://github.com/tseyanglim/CovidRiskResponse.

Figure S2 shows 90% credible intervals estimated for each country for the two main outcome measures, quasi-equilibrium normalized contact rate (g^{eq}) and quasi-equilibrium daily death rate per million (d_{NM}^{eq}).

Figure S3 shows reported daily death rates per million against change in visits to workplaces and retail & recreation venues respectively, relative to pre-pandemic levels, averaged over 180 days from 05 June 2020-02 December 2020. (The figure showing the combined index is in the main paper.) The correlation between deaths and relative daily visits is non-positive in all cases: Pearson's R^2 for averaged index = -0.371 (p = 0.0002); workplaces = -0.516 (p = 1.01E-07); retail & recreation venues = -0.249 (p = 0.016).

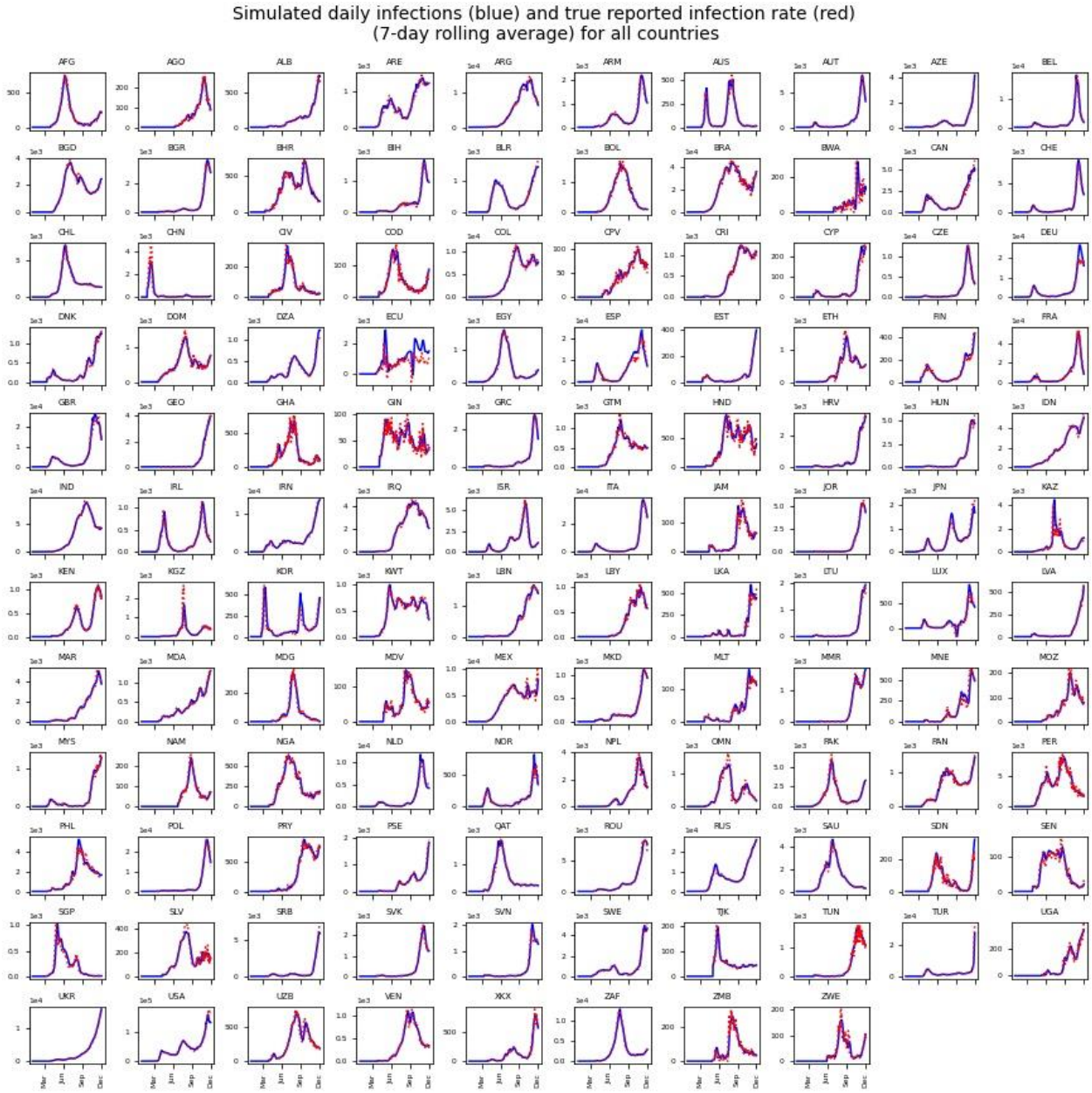

Figure S1 - Comparison of simulated infection rates with data across all 118 countries

Table S1 - Summary statistics of estimated parameter values

Parameter	Symbol	Mean	StDev	Median	Med. IQR
Reference effective contact rate	$\beta 0$	0.17	0.034	0.16	0.008
Initial responsiveness	$\alpha 0$	3.87	4.01	1.91	0.97
Final responsiveness	αf	1.46	2.79	0.19	0.064
Responsiveness inflection point	t0	197	84	211	13
Responsiveness scaling factor	θ	16.1	22.0	5.1	5.4
Time to upgrade risk	λU	12.2	9.8	8.9	3.9
Time to downgrade risk	λD	58	38	61	11
Death underreporting multiplier	γD	2.52	1.29	2.35	1.66
Likelihood scaling factor	ϵ	0.058	0.150	0.022	0.004

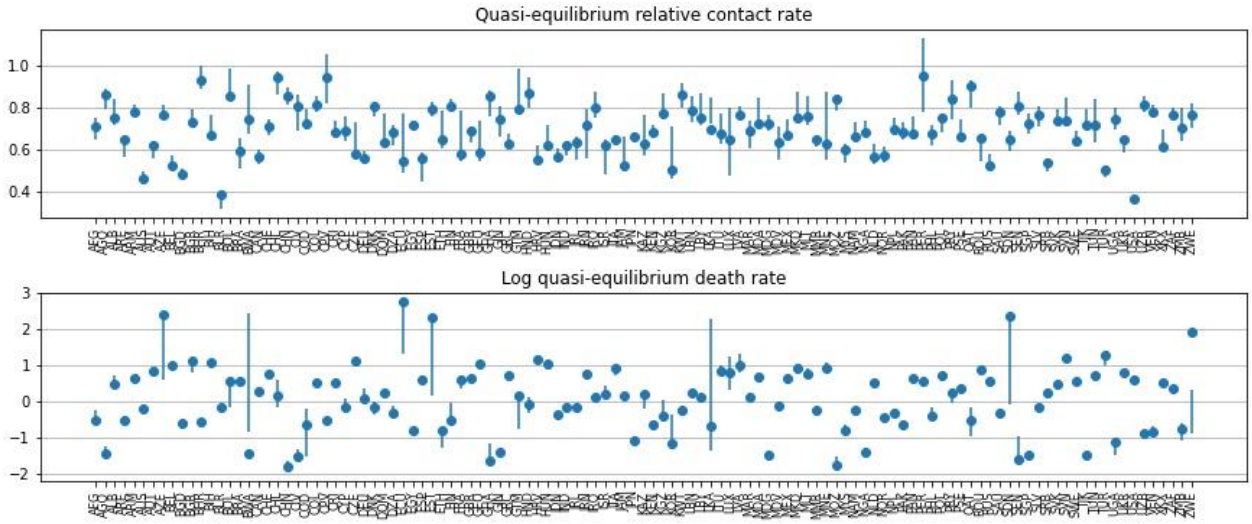

Figure S2 - 90% credible intervals for estimates of normalized contact rate and log10 daily deaths per million in quasi-equilibrium.

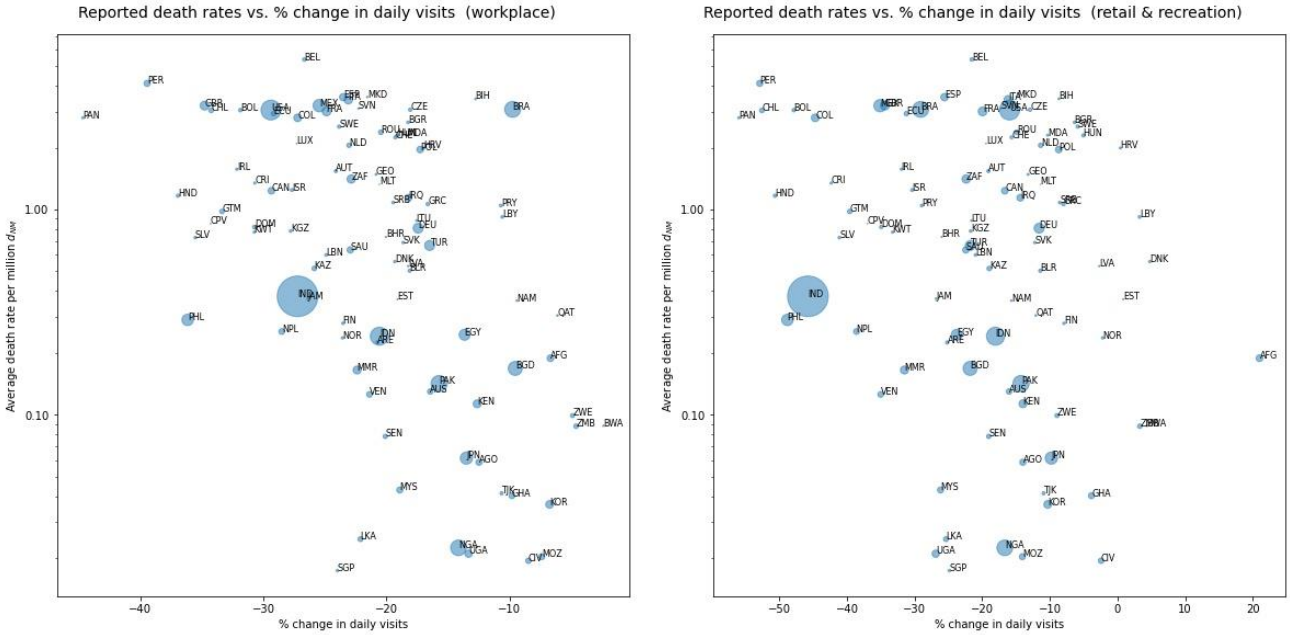

Figure S3 – Reported daily death rates per million against change in daily visits to workplaces (left) and retail & recreation venues (right) relative to pre-pandemic levels, averaged over the last 180 days from 05 June 2020-02 December 2020.

S4 – Sensitivity results

Disease Duration

We specify the average disease duration (τ) at 10 days, constant across all countries. This duration is consistent with prior findigns (He et al. 2020, Wolfel et al. 2020). To test for sensitivity to this parameter, we re-ran model estimation and analysis with τ = 8 and 14 days.

Figure S4 and Figure S5 show the main result for τ = 8 and 14 days respectively. The primary insight has not changed – expected deaths and normalized contact rates in quasi-equilibrium conditions have no positive correlation (for τ = 8 and 14 days respectively, Pearson's r = -0.044, p = 0.647 and r = 0.099, p = 0.303; for $\log(d_{NM}^{eq})$, r = -0.130, p = 0.177 and r = -0.238, p = 0.012), with if anything a slight negative correlation as per the main result.

The model is still able to fit the data reasonably well with changes in disease duration. Table S2 and Table S3 summarise estimated parameter values with τ = 8 and 14 days respectively. On average, reducing τ to 8 days results in a 10.0% absolute change in estimated parameter values, while increasing it to 14 days results in a 7.4% absolute change. The fit between simulated infections and data deteriorates slightly at τ = 14 days (R^2 = 0.930, MAEN = 14.7%) compared to baseline (R^2 = 0.936, MAEN = 13.2%). Fit improves slightly at τ = 8 days (R^2 = 0.950, MAEN = 11.5%). The primary driver of infection rates is the number of currently infected people, which is calculated exogenously from the data based on the specified disease duration. As such, some inverse relationship between quality of fit and disease duration is to be expected, as shorter durations allow autocorrelation in the [smoothed] infection data to exert a stronger influence on the accuracy of model predictions.

These results indicate that both overall model performance, and more importantly, the main results of this analysis, are robust to alternative specifications of average disease duration within a broadly reasonable range.

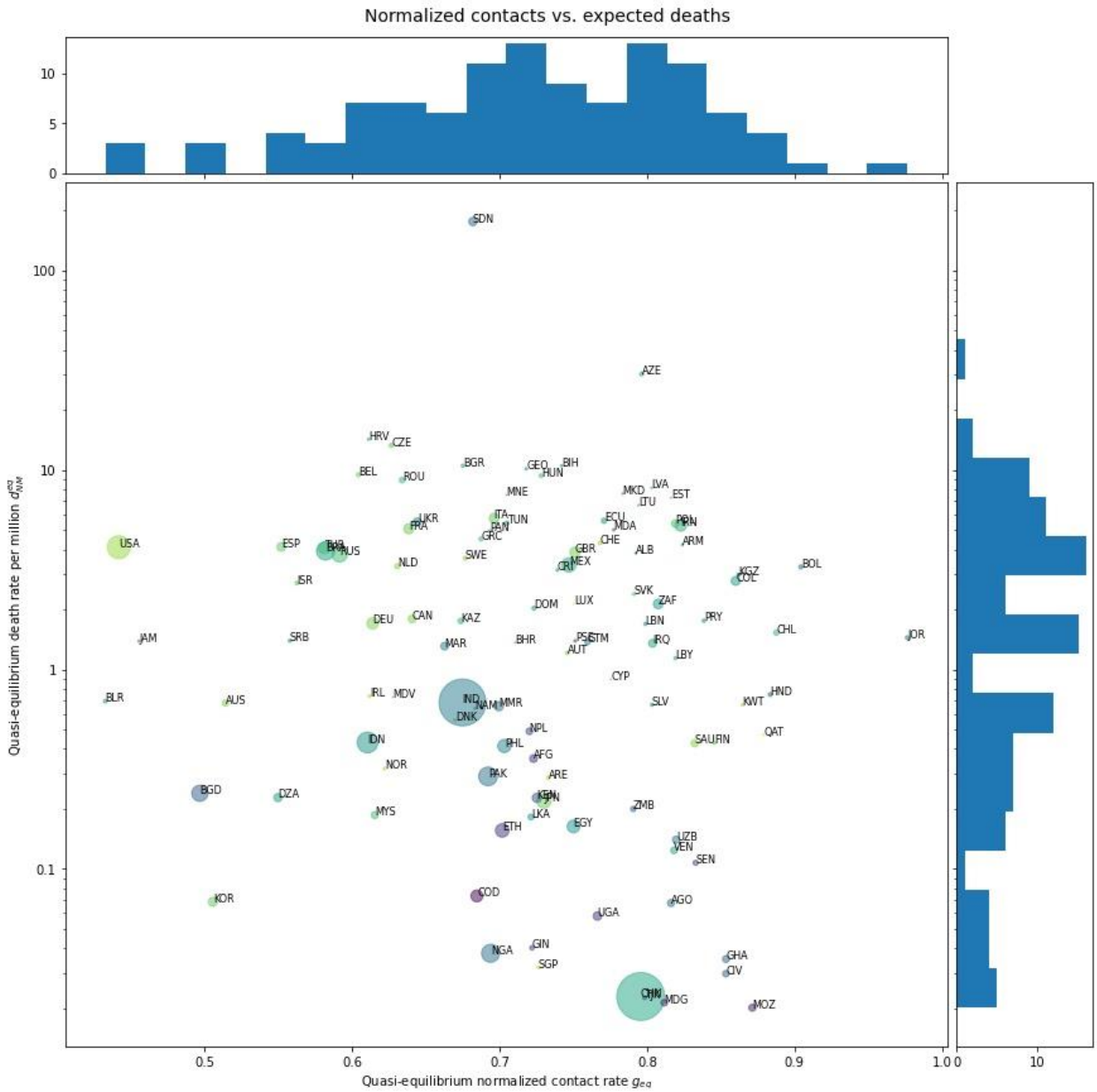

Figure S4 - Normalized contacts vs. expected deaths for $\tau = 8$ days

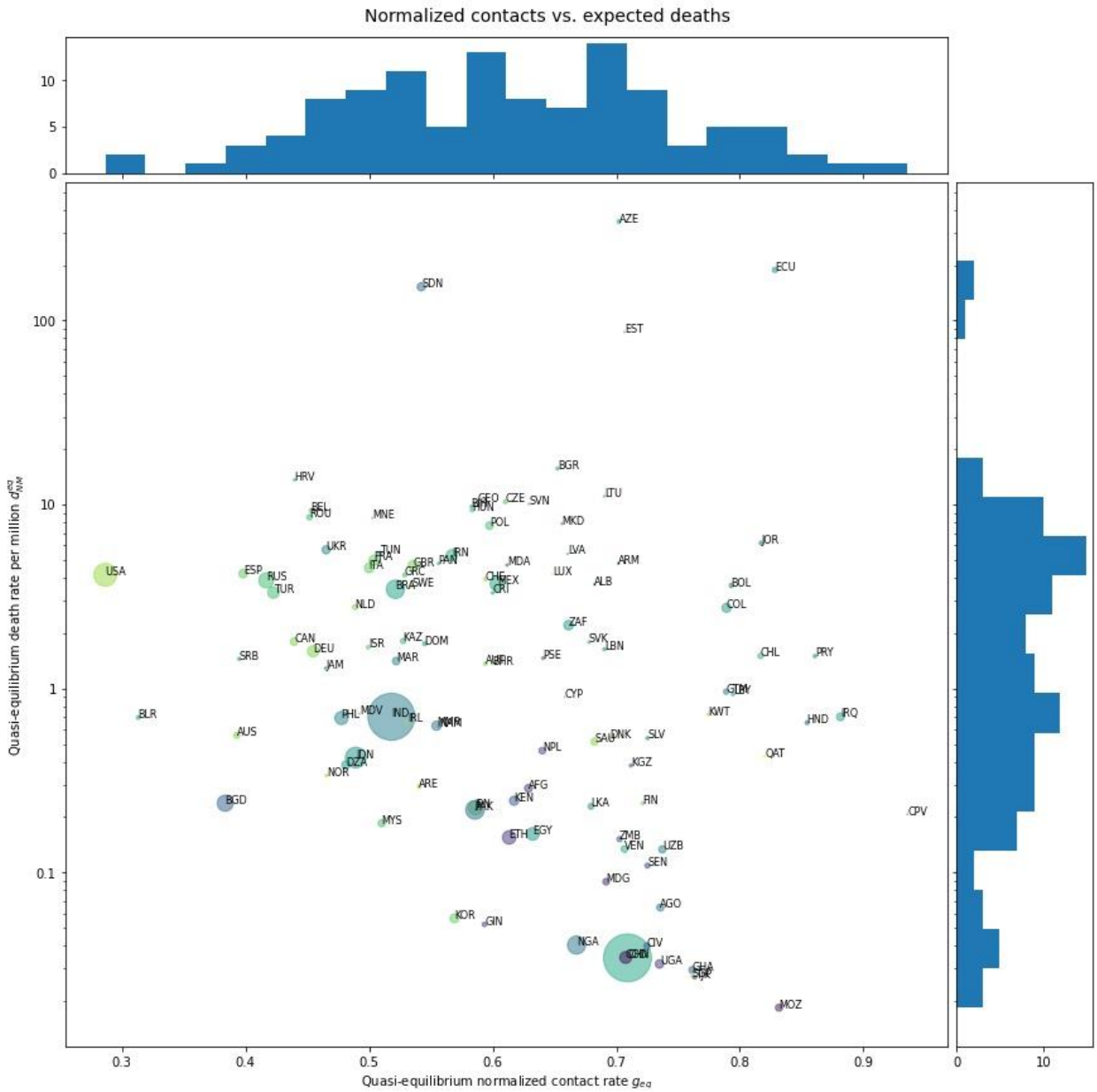

Figure S5 - Normalized contacts vs. expected deaths for $\tau = 14$ days

Table S2 - Summary of parameter estimates for τ = 8 days, with change in mean & median estimates

Parameter	Symbol	Mean	Change	Median	Change
Reference effective contact rate	$\beta 0$	0.20	0.187	0.19	0.195
Initial responsiveness	$\alpha 0$	4.30	0.111	2.12	0.109
Final responsiveness	αf	1.30	-0.114	0.21	0.098
Responsiveness inflection point	t0	190	-0.031	197	-0.068
Responsiveness scaling factor	θ	14.1	-0.127	5.0	-0.012
Time to upgrade risk	λU	11.6	-0.052	7.4	-0.175
Time to downgrade risk	λD	60	0.036	63	0.030
Death underreporting multiplier	γD	2.42	-0.039	2.21	-0.059
Likelihood scaling factor	ϵ	0.046	-0.202	0.017	-0.205

Table S3 - Summary of parameter estimates for τ = 14 days, with change in mean & median estimates

Parameter	Symbol	Mean	Change	Median	Change
Reference effective contact rate	$\beta 0$	0.14	-0.16	0.13	-0.174
Initial responsiveness	$\alpha 0$	3.95	0.02	1.70	-0.109
Final responsiveness	αf	1.65	0.13	0.35	0.848
Responsiveness inflection point	t0	201	0.02	214	0.016
Responsiveness scaling factor	θ	13.3	-0.18	5.0	-0.013
Time to upgrade risk	λU	12.7	0.04	10.3	0.160
Time to downgrade risk	λD	59	0.02	61	0.007
Death underreporting multiplier	γD	2.66	0.06	2.85	0.214
Likelihood scaling factor	ϵ	0.060	0.04	0.030	0.386

Estimation without behavioural response

We estimate the model with the endogenous behavioural response deactivated, i.e. $\alpha = 0$. In the absence of behavioural response, the fit of simulated infections to data deteriorates by 38% (R^2 = 0.914, MAEN = 18.2%), as expected, indicating that the behavioural response mechanism does improve the quality of fit. As the primary driver of infection rates is the number of currently infected people, which is calculated exogenously from the data, overall model fit remains notably good.

S5 – Model equations listing

1) AdjIFR[Rgn] = GET VDF CONSTANTS('InputConstants.vdf', 'AdjIFR[Rgn]', 1)
2) alp[Rgn] = 0.1 This parameter is 1 over the number of failures in negative binomial before experiment is stopped. A value between 0 and 1 (excluding zero) is legitimate calibraiton parameters here.
3) alpha[Rgn] = alpha 0[Rgn] + 1 / (1 + exp (timesens[Rgn])) * (alpha f[Rgn] - alpha 0[Rgn])
4) alpha 0[Rgn] = 1
5) alpha f[Rgn] = 2
6) BaseIFR = 0.005
7) beta[Rgn] = 0.1
8) CumulativeDpm[Rgn] = INTEG(DeathsOverTime[Rgn] , 0)
9) DataFlowOverTime[Rgn] = if then else (new cases[Rgn] = :NA:, :NA:, new cases[Rgn])
10) DataIncluded[Rgn] = 1
11) DataStartTimeCases[Rgn] = INITIAL(GET DATA FIRST TIME (new cases[Rgn]))
12) DataStartTimeDeaths[Rgn] = INITIAL(GET DATA FIRST TIME (new dpm[Rgn]))
13) DeathReportingRatio[Rgn] = 500
14) DeathsOverTime[Rgn] = if then else (Time < DataStartTimeDeaths[Rgn] , 0, new dpm interpolated[Rgn])
15) DeathsOverTimeRaw[Rgn] = if then else (new dpm[Rgn] = :NA:, :NA:, new dpm[Rgn])
16) Di[Rgn] = DataFlowOverTime[Rgn]
17) DiseaseDuration = 10
18) dn[Rgn] = SMOOTH N (DeathsOverTime[Rgn] , if then else (dn[Rgn] < DeathsOverTime[Rgn] , PMean[Rgn] , PMeanRelax[Rgn]) ,0, PMeanOrder)
19) eps = 0.01
20) eqDeath[Rgn] = ZIDZ (ln (beta[Rgn] * DiseaseDuration * SFrac[Rgn]) , alpha[Rgn])
21) FINAL TIME = 334 The final time for the simulation.
22) g death[Rgn] = exp (- alpha[Rgn] * dn[Rgn])
23) IFR[Rgn] = INITIAL(if then else (AdjIFR[Rgn] = -1, BaseIFR , AdjIFR[Rgn])) Note: -1 is placeholder value for missing data in InputConstants.vdf
24) inf exp[Rgn] = beta[Rgn] * roll[Rgn] * g death[Rgn] * SFrac[Rgn]
25) InfShift[Shft] := - Shft
26) INITIAL TIME = 0 initial time for the simulation.
27) Mu[Rgn] = Max (eps , inf exp[Rgn])
28) NBL1[Rgn] = if then else (DataFlowOverTime[Rgn] = 0, - ln (1 + alp[Rgn] * Mu[Rgn]) / alp[Rgn] , 0) This is the part of negative binomial distribution calcualted when outcomes are zero.
29) NBL2[Rgn] = if then else (DataFlowOverTime[Rgn] > 0, GAMMA LN (Di[Rgn] + 1 / alp[Rgn]) - GAMMA LN (1 / alp[Rgn]) - GAMMA LN (Di[Rgn] + 1) - (Di[Rgn] + 1 / alp[Rgn]) * ln (1 + alp[Rgn] * Mu[Rgn]) + Di[Rgn] * (ln (alp[Rgn]) + ln (Mu[Rgn])) , 0) This is the second piece in the loglikelihood for negative binomial which only applies to non-zero data points.
30) NBL3[Rgn] = if then else (Di[Rgn] > 0, - GAMMA LN (Di[Rgn] + 1) - (Di[Rgn] + 1 / alp[Rgn]) * ln (1 + alp[Rgn] * Mu[Rgn]) + Di[Rgn] * (ln (alp[Rgn]) + ln (Mu[Rgn])) , 0)
31) NBLLFlow[Rgn] = (NBL1[Rgn] + NBL2[Rgn]) * DataIncluded[Rgn]
32) new cases[Rgn] :RAW:
33) new dpm[Rgn] :RAW:
34) new dpm interpolated[Rgn] := new dpm[Rgn]
35) PMean[Rgn] = 5
36) PMeanOrder = 2
37) PMeanRelax[Rgn] = 20
38) Pssn : (p1-p100)
39) Re[Rgn] = beta[Rgn] * g death[Rgn] * DiseaseDuration * SFrac[Rgn]
40) Rgn : AFG, AGO, ALB, ARE, ARG, ARM, AUS, AUT, AZE, BEL, BGD, BGR, BHR, BIH, BLR, BOL, BRA, BWA, CAN, CHE, CHL, CHN, CIV, COD, COL, CPV, CRI, CYP, CZE, DEU, DNK, DOM, DZA, ECU, EGY, ESP, EST, ETH, FIN, FRA, GBR, GEO, GHA, GIN, GRC, GTM, HND, HRV, HUN, IDN, IND, IRL, IRN, IRQ, ISR, ITA, JAM, JOR, JPN, KAZ, KEN, KGZ, KOR, KWT, LBN, LBY, LKA, LTU, LUX, LVA,

MAR, MDA, MDG, MDV, MEX, MKD, MLT, MMR, MNE, MOZ, MYS, NAM, NGA, NLD, NOR, NPL, OMN, PAK, PAN, PER, PHL, POL, PRY, PSE, QAT, ROU, RUS, SAU, SDN, SEN, SGP, SLV, SRB, SVK, SVN, SWE, TJK, TUN, TUR, UGA, UKR, USA, UZB, VEN, XKX, ZAF, ZMB, ZWE

41) roll[Rgn] = if then else (Time < DataStartTimeCases[Rgn] , 0, sum (SelectRoll[Shft!] * ShiftedInfection[Rgn,Shft!]))
42) SAVEPER = TIME STEP [0,?] The frequency with which output is stored.
43) SelectRoll[Shft] = if then else (Shft > DiseaseDuration , 0, 1)
44) Series : Infection
45) SFrac[Rgn] = Max (1e-06, 1 - (CumulativeDpm[Rgn] * DeathReportingRatio[Rgn] / IFR[Rgn]) / 1e+06)
46) Shft : (S1-S20)
47) ShiftedInfection[Rgn,Shft] := TIME SHIFT (new cases[Rgn] , InfShift[Shft])
48) t0[Rgn] = 20
49) theta[Rgn] = 1
50) TIME STEP = 1 [0,?] The time step for the simulation.
51) timesens[Rgn] = MIN (50, - (Time - t0[Rgn]) / theta[Rgn])

References

Dong E, Du H, Gardner L (2020) An interactive web-based dashboard to track COVID-19 in real time. *Lancet Infect Dis* 20(5):533-534.

He X, Lau EHY, Wu P, Deng X, Wang J, Hao X, Lau YC, et al. (2020) Temporal dynamics in viral shedding and transmissibility of COVID-19. *Nat Med* 26(5):672-675.

Rahmandad H, Lim TY, Sterman J (2020) Estimating COVID-19 under-reporting across 86 nations: implications for projections and control. *Available at SSRN 3635047*.

Roser M, Ritchie H, Ortiz-Ospina E, Hasell J (2020) Coronavirus pandemic (COVID-19). *Our World in Data*.

Verity R, Okell LC, Dorigatti I, Winskill P, Whittaker C, Imai N, Cuomo-Dannenburg G, Thompson H, Walker PG, Fu H (2020) Estimates of the severity of coronavirus disease 2019: a model-based analysis. *The Lancet infectious diseases*.

Vrugt JA, Ter Braak C, Diks C, Robinson BA, Hyman JM, Higdon D (2009) Accelerating Markov chain Monte Carlo simulation by differential evolution with self-adaptive randomized subspace sampling. *International Journal of Nonlinear Sciences and Numerical Simulation* 10(3):273-290.

Wolfel R, Corman VM, Guggemos W, Seilmaier M, Zange S, Muller MA, Niemeyer D, et al. (2020) Virological assessment of hospitalized patients with COVID-2019. *Nature* 581(7809):465-469.

World-Bank (2014) World development indicators.